

Periodic drag force and particle size measurement in a double ring electrodynamic trap

G. Göbel,^{a)} Th. Wriedt, and K. Bauckhage

Department of Chemical Engineering, University of Bremen, Badgasteiner Strasse 3, D-28359 Bremen, Germany

(Received 26 March 1997; accepted for publication 14 May 1997)

A simple method to determine the size of a spherical particle in an electrodynamic trap from its dynamic behavior is introduced. Contrary to common usage of electrodynamic traps, gravity is not compensated completely. The resulting oscillatory trajectory is phase shifted with respect to the driving ac field of the trap. A light barrier setup is sufficient to determine the phase lag. An analytical solution is available in closed form to yield the particle diameter from the measured phase lag. Numerical trajectory simulations support this solution. Our method is independent of the optical properties of the particle. Only the viscosity of the surrounding gas and the particle mass density have to be known for data evaluation. © 1997 American Institute of Physics.

[S0034-6748(97)05108-3]

I. INTRODUCTION

Electrodynamic levitation (also called trap, balance, or chamber) is a well established technique for studying the physics of single aerosol particles¹⁻⁵ and particle clouds.⁶ An electrically charged particle is carried against gravity by means of a dc field. An additional ac field provides a dynamic trapping force. This allows experiments to be performed under ideal circumstances. Comprehensive reviews of this topic are given by Bar-Ziv Sarofim⁷ and by Davis.⁸

The size of a levitated particle is one of its most striking parameters. Most of the physical (optical, mechanical, or thermodynamical) properties of an individual particle are dominated by the size. Therefore sizing techniques have accompanied the evolution of particle traps.^{4,9} Optical techniques (direct reading, elastic light scattering) are often employed. But for data evaluation of such measurements the optical properties of the particle have to be known. In some applications (particle heating, phase transitions, chemical reactions) the index of refraction even changes during the experiment. Optical techniques also suffer from the fact that the underlying light scattering calculations assume a spherical particle shape. Thus, their reliability decreases strongly, if solid particles—which are seldom spherical—are the subject of investigation.

The measurement of the drag force parameter C_D of a levitated particle offers the possibility of determining its size independent of knowledge of its optical properties. The drag force due to air friction depends mainly on the relative velocity between the particle and the surrounding gas, as well as the particle size. Thus, drag force measurements can be employed to obtain the particle size. Early examples based on this idea are the work by Bar-Ziv *et al.*¹⁰ or Davis *et al.*,¹¹ who imposed an additional air flow onto a levitated particle. The change in the dc voltage that is necessary to compensate the drag force, can be evaluated in order to obtain the particle size. Sageev *et al.*¹² switched off the ac voltage for a short length of time and determined the steady state particle

velocity by means of a photomultiplier with a spatial filter in front.

Maloney *et al.*¹³ reported a different approach to determine the drag force parameter. A transient particle trajectory is generated by rapidly changing the dc voltage (short dc step) of the trap. The trajectory, governed both by the electrical fields inside the trap and the damping, is recorded against time by means of an optical sensor. A numerical algorithm for the simulation of particle trajectories is employed iteratively. The particle diameter and thus the drag force are adjusted to find optimal agreement between the calculated and the detected trajectory.

In this article we show that particle size measurements, based on the drag force in an electrodynamic trap, can be performed in a much easier way by employing a periodic particle motion rather than a transient process. We do not compensate for gravity completely by the electrical dc field. This leads to an oscillatory particle movement in the vertical direction around a point outside the center of the trap. The frequency of the oscillation is the frequency of the applied ac field. The drag force leads to an additional phase lag between the external driving force (ac voltage) and the particle's response. This phase lag is known to be a function of the air viscosity η , the driving frequency ω and ρd^2 (ρ : particle mass density, d : diameter of a spherical particle) only. We use a simple experimental setup based on a photoelectric barrier to determine the phase lag. The relationship between the phase lag and the particle size is available in closed form. No synchronized trajectory detection, no trajectory calculation and no iterative parameter adjustment in a fitting routine are necessary to yield the particle diameter.

The solution for the phase shifted motion of a damped particle inside an electrodynamic trap, used to obtain the particle diameter from the measured phase lag, was published in 1985 by Arnold and Hessel¹⁴ but was not used for size measurements. Phase lag (sometimes also called relaxation time) measurements similar to our proposed method have been performed in an apparatus called E-SPART.¹⁵ An acoustic or electrodynamic driving force of high frequency was applied to accelerate particles perpendicular to their

^{a)}Electronic mail: gerhard@iwt.uni-bremen.de

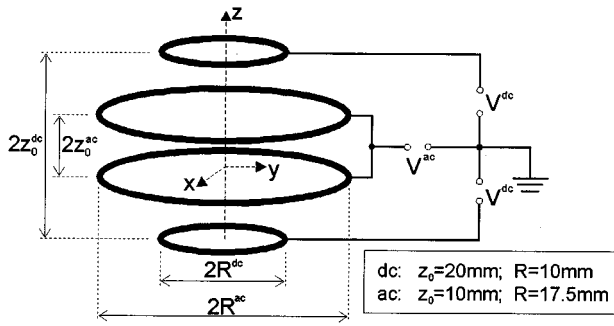


FIG. 1. Setup scheme of the double ring electrodynamic particle trap together with the geometrical data.

main velocity component in an aerosol stream. Relaxation time measurements based on air damping have also been performed in optical traps.¹⁶

II. ELECTRODYNAMIC DOUBLE RING PARTICLE TRAP

A. Trap setup

We use a simple double ring electrodynamic trap¹⁷ in our experiments. The trap is built of four ring electrodes (Fig. 1). The rings are arranged parallel with their centers coinciding with the vertical (z) axis of symmetry. This z axis defines the direction of gravity. The end electrodes are supplied with up to 300 V dc voltage, normally of opposing polarity. Both polarity and magnitude of each dc electrode potential can be adjusted individually. The center electrodes carry an ac voltage (max 5 kV, $46 \text{ Hz} < \omega/2\pi < 1 \text{ kHz}$) of equal polarity. For all further considerations we assume that both ac and both dc electrodes are identical in size and that they are positioned symmetrically. For details on particle charging and trapping procedures for both solid and liquid particles, we refer to previous articles on that topic.^{14,18}

B. Electrical field inside the trap

Knowledge of the electrical field inside the particle trap is necessary for the calculations and subsequent analysis of particle trajectories. Furthermore, it is desirable to obtain the trap constant C_0 on a theoretical basis. C_0 is the scaling factor between the applied dc voltage V^{dc} and the resulting dc field strength $E_z^{\text{dc}}|_0$ at the center of the trap.

The electrical potential of a charged ring (ring material diameter b) of radius R , placed parallel to the x - y axis of a coordinate system at a vertical position z_0 , is obtained by solving the Laplace equation. According to the symmetry of the problem a cylindrical coordinate system is chosen. The solution—basically a complete elliptic integral of the first kind—was published and discussed in detail by Davis *et al.*¹⁹ Elliptic integrals of the first kind can be evaluated numerically for arbitrary arguments with a standard routine *cel*.²⁰ For small arguments we use a power series expansion.²¹ As opposed to Davis *et al.*,¹⁹ we do not differentiate the elliptic integral itself but instead differentiate its power series expansion to yield electric field strengths. The total dc and ac electric fields at a time t are obtained by a linear superposi-

tion of the individual ring contributions. As the electric field distribution is smooth at the center of the trap, we can achieve an approximative analytical solution for the electric field strengths. We restrict ourselves to positions along the z axis and terminate the series for the elliptic integral after the second term to find

$$E_z^{\text{ac}} \approx K_e \frac{z}{\chi^3} \left(1 - 3 \frac{z_0^2}{\chi^2} \right) e^{-i\omega t}, \quad (1)$$

$$E_z^{\text{dc}} \approx K_e \frac{z_0}{\chi^3} \left(1 - \frac{z^2}{\chi^2} \right), \quad (2)$$

with

$$\chi^2 = R^2 + z_0^2$$

and

$$K_e = \frac{Q}{2\pi\epsilon_0}.$$

R and z_0 are the radius and the vertical position of the ac and dc rings, respectively, while ϵ_0 is the vacuum permittivity. We see that the dc field is independent of z to first order approximation. Thus gravity is compensated for over the center of the trap if the dc voltage is adjusted accordingly. Contrary to this the strength of the ac field changes linearly with z . It vanishes only at the center of the trap. In accordance with Ref. 19 we find for the trap constant C_0 :

$$C_0 \propto \frac{z_0^2}{\sqrt{z_0^2 + R^2}}^3. \quad (3)$$

Q in Eq. (2) is the so-called generating charge on the ring. According to Davis *et al.*¹⁹ Q can be found by forcing the potential at the ring surface to equal the applied voltage. We performed additional electric field calculations by means of MAFIA,²² which is a commercial electromagnetic solver (time domain, finite differences) and found general agreement with the approximative solution given above.

More precise approximations for the course of the electric fields can be obtained by taking into account higher order terms of the elliptic integral series expansion. This was performed and the results were published for a variety of trap configurations different from our double ring trap by Hartung and Avedisian.²³

III. PARTICLE TRAJECTORY CALCULATION

An arbitrary shaped particle (mass m , density ρ) can be characterized by a volume equivalent sphere diameter d_V ($m = \pi/6 \rho d_V^3$). The drag force on a particle moving with velocity v in a fluid of density ρ_g and viscosity η depends strongly on the particle Reynolds number Re_p :

$$Re_p = \frac{\rho_g d_V v}{\eta}. \quad (4)$$

For Reynolds numbers below $Re_p < 0.1$ the drag force on an arbitrary shaped particle is described by the following extended version of Stokes law:

$$F_D = \frac{3\pi\eta d_V K v}{C_c} = \frac{C_D v}{C_c}. \quad (5)$$

As we consider only particle diameters clearly larger than the free mean path of the gas molecular motion, the Cunningham slip correction factor, C_c , equals 1 and is omitted in the following. $C_D = 3\pi\eta d_V K$ is called the drag force coefficient. Confusion can arise from the fact that a similar symbol, the drag coefficient C_d , is commonly used in Newton's law:

$$F_D = C_d \frac{\pi}{8} \rho_g d_V^2 v^2, \quad (6)$$

which can be simplified to Eq. (5) for laminar flow ($C_d = 24/Re_p$). The dynamic shape correction factor K of a nonspherical particle was derived by Leith:²⁴

$$K = \frac{1}{3} + \frac{2}{3} \frac{d_s}{d_n}. \quad (7)$$

d_s and d_n are equivalent sphere diameters with respect to the total surface of the particle and its projected area to a plane perpendicular to the flow direction. Although Eq. (7) is valid for arbitrarily shaped particles, corrections based on a calibration to experimental data are recommended for strong deviations from a spherical particle shape.²⁴ For a sphere of diameter $d_V = d$ the dynamic shape correction factor reduces to $K = 1$.

We can now describe the three dimensional motion of a particle (electric charge q) within the electrodynamic trap by the following differential equation:

$$m\ddot{\vec{r}} = -mg\vec{e}_z - C_D\dot{\vec{r}} + q\vec{E}^{ac} + q\vec{E}^{dc}. \quad (8)$$

\vec{e}_z is the unit vector pointing along the direction of gravity, and g is the gravitational acceleration. The drag force is assumed to act in the direction of $\dot{\vec{r}}$. This is valid even for nonspherical particles, as long as the flow can be regarded as laminar and no particle alignment takes place.²⁵

While E_z^{dc} is constant within the area of interest [Eq. (2)], E_z^{ac} is proportional to z to first order approximation [Eq. (1)] for particle positions close to the trap nullpoint:

$$E_z^{ac} = \alpha \cdot z \cdot e^{-i\omega t},$$

with

$$\alpha = \frac{K_e}{\chi^3} \left(1 - 3 \frac{z_0^2}{\chi^2} \right). \quad (9)$$

This makes Eq. (8) a Mathieu type differential equation in the z direction, which is commonly solved numerically. Analytical solutions for Eq. (8) are available only in form of power series expansions,^{7,26} the method of continued fractions,²⁷ or by applying approximations for special cases of particle motion. Both a numerical solution for arbitrary trajectories and an approximative analytical solution for the case of an oscillating particle will be presented in the following.

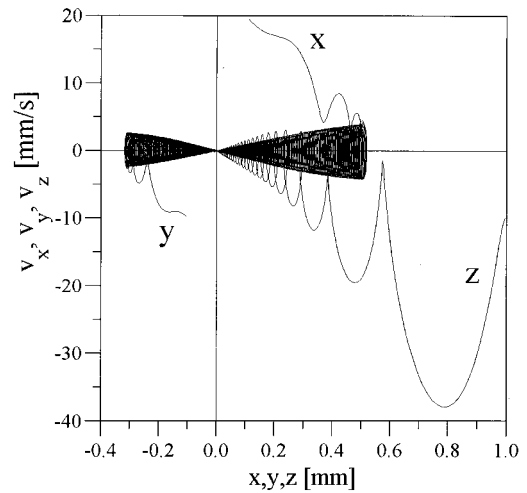


FIG. 2. Phase plot of a 50 μm particle trajectory in an electrodynamic trap ($V^{ac} = 3$ kV at $\omega/2\pi = 50$ Hz, $V^{dc} = \pm 100$ V). The initial values for position and velocity are given in the text.

A. Numerical trajectory integration

We start with the description of a numerical solution of Eq. (8). This enables us to simulate particle trajectories for arbitrary initial particle positions and velocities without any limiting approximation. Eq. (8) can be treated as an initial value problem and can be solved with a finite difference integration method. We use a Runge–Kutta algorithm with an adaptive step size control.²⁰ The calculations are performed in Cartesian coordinates in three dimensional geometry.

The result of such a simulation for a $d = 50$ μm particle of density $\rho = 2.5$ g/cm^3 is depicted in Fig. 2. A dc voltage of 100 V was selected. Thus the particle charge was calculated accordingly to compensate for gravity completely ($q = 3.807 \times 10^6 e$). The initial values for the particle position and velocity were chosen different from zero ($\vec{r}_0 = (0.1 | -0.1 | 1.0)$ mm, $\dot{\vec{r}}_0 = (20 | -10 | -10)$ mm/s). For each Cartesian coordinate the phase space diagram (v_x vs x) is depicted for a time period of 5 s. For all components, conical structures can be seen. They are composed of elliptical courses with decreasing radii that tend toward the center of the trap. This corresponds to the phase space diagram of a damped oscillation. While the trapping is moderate in the x and y directions, we observe a much faster decrease of the z coordinate of the particle position. The center area (± 12 μm) of the trap is shown enlarged in Fig. 3 for a detailed study of the trapping process. Here only the z coordinate is depicted for reasons of clarity. An overshooting in the particle motion can be seen due to the momentum of the particle in the z direction. With increasing distance from the trap center the oscillation amplitude increases linearly due to the z dependence of E_z^{ac} . At $z \approx -10$ μm the movement of the oscillation center comes to rest before a moderately damped drift back to the trap center takes place.

B. Analytical solution

If gravity is not compensated completely by the dc field, a levitated particle oscillates in the vertical direction. As

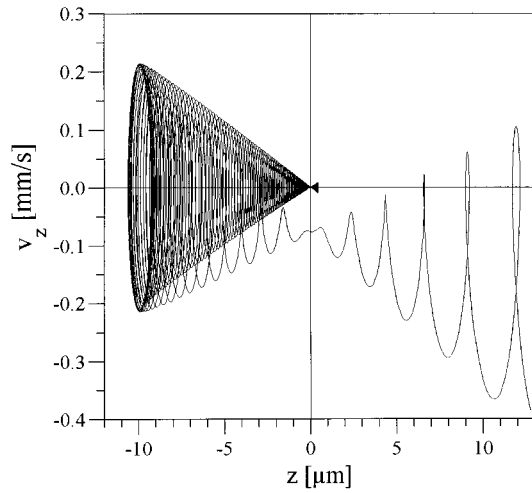


FIG. 3. Enlarged phase plot trajectory depiction of the center area ($-12 \mu\text{m} < z < 12 \mu\text{m}$) of Fig. 2. Only the z coordinate is shown. An overshwing can be seen before the oscillation center $\langle z \rangle$ comes to rest and slowly moves back toward the trap center.

there is no driving force component in the horizontal direction, any initial trajectory component is damped out. For the steady state solution we can assume a one dimensional motion. According to the expected vertical oscillation we split the particle motion into two components:

$$z(t) = \langle z \rangle + \tilde{\zeta} \cdot e^{-i\omega t}. \quad (10)$$

The position of the oscillation midpoint $\langle z \rangle$ is to change only over timescales much larger than the oscillation period and is assumed to be constant in the following. $\tilde{\zeta}$ is the complex valued oscillation amplitude. Although this kind of separation has been used repeatedly,^{14,28} a careful examination of the validity of this assumption is advised. If the trap parameters are chosen to yield an oscillation amplitude ζ much smaller than $\langle z \rangle$,

$$\zeta \ll \langle z \rangle$$

with

$$\zeta = |\tilde{\zeta}|, \quad (11)$$

we can assume that the change in the ac field strength is negligible along the amplitude of the oscillation and can therefore replace z in Eq. (9) by $\langle z \rangle$. The solution for the resulting one dimensional equation of motion for ζ was given by Arnold and Hessel¹⁴ as

$$\tilde{\zeta} = \frac{-\alpha q \langle z \rangle}{m\omega^2 + i\omega C_D}. \quad (12)$$

The phase lag between the driving ac field and the particle motion is

$$\tan \Phi = \frac{C_D}{m\omega} = \frac{18\eta K}{d_V^2 \rho \omega}. \quad (13)$$

Φ is only a function of the drag force coefficient to mass ratio C_D/m for a fixed ac frequency ω . As we restrict ourselves to spherical particles within the scope of this article, $K=1$ and the C_D/m ratio reduces to $18\eta/(\rho d^2)$. As the

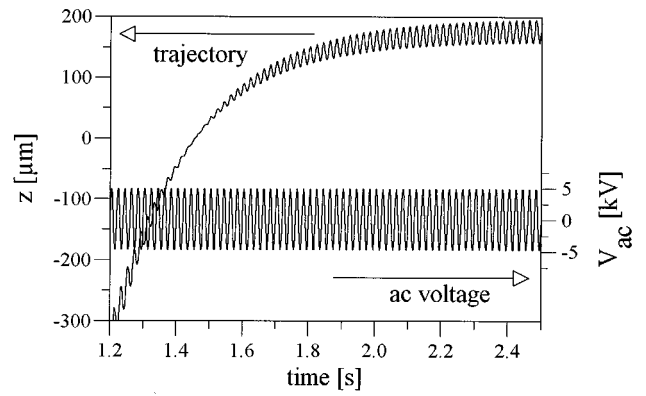


FIG. 4. Example of a numerically calculated particle trajectory ($d=30 \mu\text{m}$, $\omega=314 \text{ Hz}$, $\vec{r}_0=(10|-10|100)\mu\text{m}$, $\dot{\vec{r}}_0=(0|0|0) \text{ mm/s}$). Only the z component is depicted. In addition the driving ac voltage is shown (right axis).

viscosity η of air is well known,²⁹ d can be determined if the density ρ is available. For particle shapes other than spheres K is a second unknown quantity.

The behavior of Φ versus sphere diameter d can be explained with the size dependence of the forces acting on such a sphere. While the particle inertia is proportional to d_V^3 , the drag force is proportional only to d_V . Thus the inertia is dominant for relatively large particles. In this case the motion can be considered free of drag and the phase lag is π . With decreasing size the drag gains importance and increases the phase lag up to the limit of $\frac{3}{2}\pi$ for a drag dominated motion.

C. Numerical validation

In order to check the validity of Eq. (13) a large number of numerical trajectory calculations described in Sec. III A were performed for various particle diameters ($1.0 \mu\text{m} < d < 80 \mu\text{m}$), ac frequencies ($\omega < 1 \text{ kHz}$), and initial values \vec{r}_0 and $\dot{\vec{r}}_0$. The air viscosity ($\eta=1.74 \times 10^{-5} \text{ N s/m}^2$) and the particle density ($\rho=2.5 \text{ g/cm}^3$) were held constant. The dc voltage was shifted 1% with respect to ideal gravity compensation to yield a realistic value for the oscillation amplitude. An example trajectory (z component only) is depicted in Fig. 4 (channel 0) together with the driving ac voltage (channel 1). The phase lag Φ between both channels was evaluated by means of a fast Fourier transform (FFT) algorithm.

Fig. 5 shows the phase lag $\tan \Phi$ vs $1/\omega d^2$ in a log-log diagram. Each point represents one simulation similar to Fig. 4. As can be seen, the analytical result according to Eq. (13) (solid line) is in full agreement with the numerically obtained results.

IV. EXPERIMENTAL SETUP

The geometry of our electrodynamic double ring trap was presented in Fig. 1. The trap is surrounded by a wind shield with various laser light inlets and observation windows. The trap is mounted on a three-axis translation stage to enable precise positioning of the particle with respect to the light barrier. A Questar QM-1 telescope focused on the cen-

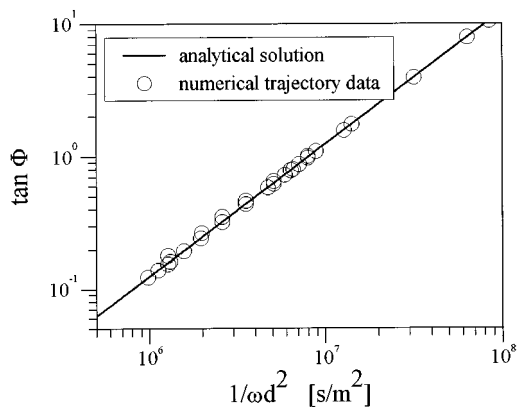


FIG. 5. Comparison between the phase lag Φ obtained by numerical trajectory simulations (\circ) and the analytical result (—); $\tan \Phi$ is depicted vs $1/\omega d^2$.

ter of the trap is a useful tool for visual observation of particle trajectories, especially during particle trapping and fine adjustment of the electrical fields. A random access light sensor (Fuga 19b, 1920×192 elements) is mounted close to the trap. Reading a single line of the sensor gives the angular scattering distribution of the levitated particle, which can be evaluated to obtain the particle diameter. Rather than performing exact Mie calculations, we use an approximative but linear relation between the particle size parameter $\alpha = \pi d/\lambda$ and the angular peak frequency for that purpose.^{30,31}

The amplitude of the oscillating particle trajectory is typically smaller than 200 μm . It can easily be adjusted by varying the electric parameters of the trap. A light barrier is used to measure the phase shift of the particle oscillation relative to the ac field. It consists of a laser beam (argon ion laser, $P = 50 \text{ mW}$ at $\lambda = 488 \text{ nm}$) and a photomultiplier tube (PMT) with a standard optical assembly (imaging system, pinhole, aperture). The scheme of this setup is depicted in Fig. 6. The laser is focused to a spot size clearly smaller than the oscillation amplitude of the particle. A typical value is $\approx 15 \mu\text{m}$. The focus is placed on an arbitrary position along the particle trajectory. The particle crosses the laser focus twice per period. The shape of the PMT signals results from the Gaussian laser beam profile and the particle velocity gra-

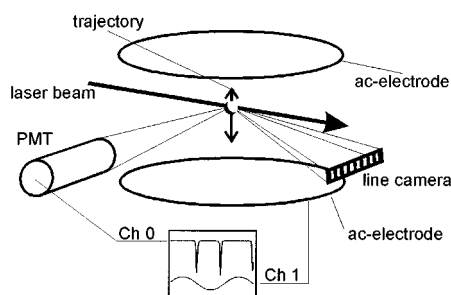


FIG. 6. Scheme of the experimental setup. A strongly focused laser beam and PMT build up a light barrier. Both the PMT signal and the ac voltage are recorded and evaluated with respect to the phase lag Φ between them. A line camera is used for angular scattering measurements to yield a reference value for the particle size. Visual observation is performed with a Questar telescope (not depicted).

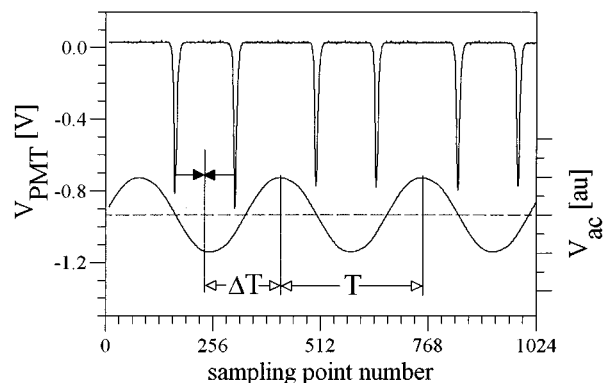


FIG. 7. Typical experimental reading of a phase lag experiment on a levitated and oscillating particle. The sampling frequency was $f_s = 60 \text{ kHz}$. The ac voltage reading (right axis) and the signal of the photomultiplier tube PMT (left axis) is depicted. The temporal difference between the peak center and the ac voltage maximum yields the phase lag $\Delta\Phi$.

dient during the laser beam crossing. For measurements close to the oscillation midpoint the signal shape is plain Gaussian.

The optical signal and the ac voltage (reduced by means of a bleeder chain) are digitized by a two channel transient recorder card and stored in a personal computer for further data evaluation. The sampling rate is chosen clearly higher than the ac frequency to ensure appropriate resolution. We use a two channel 30 MHz analog-to-digital (AD) board with a dynamic range of 12 bit. With an ac frequency below 1 kHz sampling rates of 100 kHz are sufficient. A typical reading of the two channels is depicted in Fig. 7. The temporal average between corresponding peaks in the PMT signal is equivalent to the time when the particle changes direction (extremal points of oscillation). This time has to be compared with the time when the driving ac voltage is at the extreme to yield the phase shift Φ .

The particle diameter d can in principle be obtained from a single phase lag measurement according to Eq. (13). In order to increase the quality of our result we take repeated measurements on the same particle. The ac frequency ω is changed within the available range which is mainly limited by the stability of the particle trapping. According to Eq. (13) we should yield a linear relationship if $\tan \Phi$ is plotted versus $2\pi/\omega$. The slope of the resulting straight line is given by $9\eta/(\pi\rho d^2)$ for a sphere.

The particle velocity is maximal at the center of the oscillation and given by

$$v_0 = \zeta \cdot \omega. \quad (14)$$

As we used Stoke's law for calculating the drag force on the particle in Eq. (5), we have to limit the Reynolds number to values below 0.1 for every point along the particle trajectory. This leads to the following constraint:

$$\zeta \cdot \omega < \frac{\eta}{10 d_V \rho_g}. \quad (15)$$

ρ_g is the density of the surrounding gas inside the trap. The ac frequency ω and the oscillation amplitude ζ have to be chosen with respect to Eq. (15). Thus ζ has to be decreased for high frequencies ω .

TABLE I. Physical properties of the particles and fluids used in our experiments. d_{ref} is the reference value for the particle diameter given by the manufacturer.

System	Density (g/cm ³)	d_{ref} (μm)	n_λ
Glycerin	1.23	...	1.48 ₄₈₈
PS monosphere	1.05	32.2 ± 0.6	1.61 ₄₈₈
MF monosphere	1.51	14.91 ± 0.27	1.68 ₆₃₃

If measurements are performed at higher Reynold's numbers, the drag force F_D is underestimated in Eq. (5), and so is the resulting phase lag Φ . This can be regarded as a source of systematic error. As it occurs at small values of the abscissa $2\pi/\omega$, it can be counteracted by including the limiting case,

$$\lim_{\omega \rightarrow \infty} \Phi = \pi, \quad (16)$$

as an additional constraint in the linear regression for the slope of the straight line.

V. RESULTS AND DISCUSSION

Measurements were performed on glycerin droplets and solid spheres. Table I summarizes the physical properties of the media involved. Solid monospheres from different sources (polystyrol particles from Duke Scientific and MF melamin resin particles from Micro Particles GmbH, Berlin) were employed.

Fig. 8 shows the measured phase lag $\tan \Phi$ vs $2\pi/\omega$. As described above, the ac frequency was varied for each levitated particle within the limits drawn by the empirical stability of the trap (typically $46 \text{ Hz} < \omega/2\pi < 500 \text{ Hz}$). Both the ac and the dc voltages have to be adjusted at each frequency in order to provide the desired trajectory that has a small oscillatory amplitude. As the density ρ is known for all media under consideration, we can calculate the particle diameter d from the slope m of the straight line. m in turn is evaluated by means of a linear regression.

The phase lag Φ is calculated from time period readings according to Fig. 7. The uncertainty of a single time reading σ_0 depends on the sampling frequency f_{samp} and the quality of the signal. It is in the order of the time spacing corre-

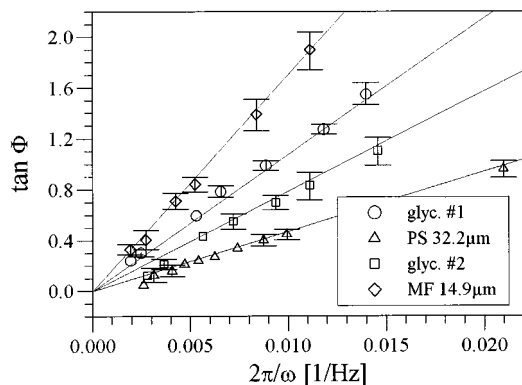


FIG. 8. $\tan \Phi$ vs $2\pi/\omega$ for glycerin droplets and various solid monospheres. The slope of the straight line is evaluated to yield the particle diameter.

TABLE II. Experimental results from phase lag measurements. The slope m of the linear regression line and the corresponding diameter d are given together with the uncertainty. The diameters d_{scat} obtained from angular scattering measurements (average value and standard deviation from ≈ 1000 readings) are also listed.

No.	System	d_{scat} (μm)	Slope (1/s)	d (μm)
1	Glycerin	20.05 ± 0.54	107.6 ± 5.9	19.4 ± 1.1
2	Glycerin	22.31 ± 0.23	78.7 ± 2.7	22.7 ± 0.7
3	PS	31.24 ± 0.40	47.2 ± 1.5	31.7 ± 0.9
4	MF	14.82 ± 0.52	176.4 ± 7.9	14.5 ± 0.7

sponding to $1/f_{\text{samp}}$. Higher resolution could be achieved by fitting an analytical function to the measured signals (i.e., a Gaussian profile for the light barrier signals and a harmonical function for the ac signal). For determination of the ac frequency $T = 2\pi/\omega$ two time readings are necessary, whereas three readings are needed to obtain the time spacing ΔT . Thus we find for the uncertainty $\sigma_{\Delta\Phi}$ of the phase lag $\Delta\Phi$:

$$\frac{\sigma_{\Delta\Phi}}{\Delta\Phi} = \sigma_0 \sqrt{\frac{3}{\Delta T^2} + \frac{2}{T^2}}. \quad (17)$$

The uncertainty in the abscissa $\sigma_{2\pi/\omega} = \sqrt{2}\sigma_0$ is negligible compared to $\sigma_{\Delta\Phi}$. Therefore only $\sigma_{\Delta\Phi}$ is depicted in Fig. 8. The uncertainty in the slope m and thus in the particle diameter d is obtained from the maximum variation of the straight line within these error bars. For all particles the relative uncertainty in $\Delta\Phi$ or d is below 6%.

In Table II the resulting diameters are given together with reference values from angular scattering measurements. Reference data are usually provided by the manufacturer of the monospheres. These values are also listed. The agreement between our phase lag results, the reference values given, and the angular scattering results is good for all particles.

We can thus suggest that the phase lag technique applied to oscillating particles in electrodynamic traps provides a simple and reliable tool for determination of the particle diameter. The measurement range is basically limited by the trapping stability. No information on the optical properties is necessary. Both the measurement and the data evaluation are much more simple than in equivalent techniques based on trajectory detection and simulation.

Our phase lag measurements are in general agreement with the reference data. In all cases the agreement is within the calculated uncertainties.

- ¹A. S. Myerson, A. F. Izmailov, and H. S. Na, *J. Cryst. Growth* **166**, 981 (1996).
- ²H. H. Blau, D. J. McCleese, and D. Watson, *Appl. Opt.* **9**, 2522 (1970).
- ³A. K. Ray, A. Souyri, E. J. Davis, and T. M. Allen, *Appl. Opt.* **30**, 3974 (1991).
- ⁴E. J. Davis and P. Ravindran, *Aerosol. Sci. Technol.* **1**, 337 (1982).
- ⁵T. L. Ward, S. H. Zhang, T. M. Allen, and E. J. Davis, *J. Colloid Interface Sci.* **118**, 343 (1987).
- ⁶R. Vehring, C. L. Aardahl, E. J. Davis, G. Schweiger, and D. S. Covert, *Rev. Sci. Instrum.* **68**, 70 (1997).
- ⁷E. Bar-Ziv and A. F. Sarofim, *Prog. Energy Combust. Sci.* **17**, 1 (1991).
- ⁸E. J. Davis, *J. Aerosol. Sci.* **26**, 212 (1997).
- ⁹A. K. Ray and R. Nandakumar, *Appl. Opt.* **34**, 7759 (1995).

- ¹⁰E. Bar-Ziv, B. D. Jones, E. R. Spjut, D. R. Dudek, A. F. Sarofim, and J. P. Longwell, *Combust. Flame* **75**, 81 (1989).
- ¹¹E. J. Davis and P. Ravindran, *Langmuir* **1**, 373 (1985).
- ¹²G. Sageev, J. H. Steinfeld, and R. C. Flagan, *Rev. Sci. Instrum.* **57**, 933 (1986).
- ¹³D. J. Maloney, L. O. Lawson, E. G. Fasching, and E. R. Monazam, *Rev. Sci. Instrum.* **66**, 3615 (1995).
- ¹⁴S. Arnold and N. Hessel, *Rev. Sci. Instrum.* **56**, 2066 (1985).
- ¹⁵R. G. Renninger, M. K. Mazumder, and M. K. Testerman, *Rev. Sci. Instrum.* **52**, 242 (1981).
- ¹⁶G. Roll, T. Kaiser, and G. Schweiger, *J. Aerosol. Sci.* **27**, 105 (1996).
- ¹⁷E. J. Davis and A. K. Ray, *J. Colloid Interface Sci.* **75**, 566 (1980).
- ¹⁸D. Lamb, A. M. Moyle, and W. H. Brune, *Aerosol. Sci. Technol.* **24**, 263 (1996).
- ¹⁹E. J. Davis, M. F. Buehler, and T. L. Ward, *Rev. Sci. Instrum.* **61**, 1281 (1990).
- ²⁰W. H. Press, B. P. Flannery, S. A. Teukolsky, and W. T. Vetterling, *Numerical Recipes in C: The Art of Scientific Computing* (Cambridge University Press, Cambridge, 1992).
- ²¹M. Abramowitz, I.A. Stegun, *Handbook of Mathematical Functions* (Dover, New York, 1970).
- ²²T. Weiland, *Int. J. Numer. Mod.* **9**, 295 (1996).
- ²³W. H. Hartung and C. T. Avedisian, *Proc. R. Soc. London, Ser. A* **437**, 237 (1992).
- ²⁴D. Leith, *Aerosol. Sci. Technol.* **6**, 153 (1987).
- ²⁵W. C. Hinds, *Aerosol Technology* (Wiley, New York, 1982).
- ²⁶E. Bar-Ziv, G. de Botton, R. H. Bar-Ziv, Y. Martsiano, and G. Ben-Dor, *Aerosol. Sci. Technol.* **14**, 127 (1991).
- ²⁷R. H. Frickel, R. E. Shaffer, and J. B. Stamatoff, Report No. ARCSL-TR-77041, Chemical Systems Laboratory, Aberdeen Proving Ground, MD, 1978.
- ²⁸R. F. Wuerker, H. Shelton, and R. V. Langmuir, *J. Appl. Phys.* **30**, 342 (1959).
- ²⁹*Handbook of Chemistry and Physics, 1913-1995* (Chemical Rubber, Boca Raton, FL, 1994).
- ³⁰J. F. Widmann and E. J. Davis, *Colloid Polym. Sci.* **274**, 525 (1996).
- ³¹S. L. Min and A. Gomez, *Appl. Opt.* **35**, 4919 (1996).